Current Applied Physics 18 (2018) 1240–1247

Contents lists available at ScienceDirect

Current Applied Physics

journal homepage: www.elsevier.com/locate/cap

Temperature dependence of the effective anisotropy in Ni nanowire arrays

Fernando Meneses[a], Silvia E. Urreta[a], Juan Escrig[b], Paula G. Bercoff[a,*]

[a] Facultad de Matemática, Astronomía, Física y Computación, Universidad Nacional de Córdoba. Instituto de Física Enrique Gaviola, CONICET. Ciudad Universitaria, Córdoba, Argentina

[b] Departamento de Física, Universidad de Santiago de Chile, USACH. Center for the Development of Nanoscience and Nanotechnology, CEDENNA. 917-0124, Santiago, Chile

ARTICLE INFO

Keywords:
Nickel nanowires
Magnetic anisotropy
Electrodeposition
Magnetization reversal modes

ABSTRACT

Magnetic hysteresis in Ni nanowire arrays grown by electrodeposition inside the pores of anodic alumina templates is studied as a function of temperature in the range between 5 K and 300 K. Nanowires with different diameters, aspect ratios, inter-wire distance in the array and surface condition (smooth and rough) are synthesized. These microstructure parameters are linked to the different free magnetic energy contributions determining coercivity and the controlling magnetization reversal mechanisms. Coercivity increases with temperature in arrays of nanowires with rough surfaces and small diameters —33 nm and 65 nm— when measured without removing the alumina template and/or the Al substrate. For thicker wires —200 nm in diameter and relatively smooth surfaces— measured without the Al substrate, coercivity decreases as temperature rises. These temperature dependences of magnetic hysteresis are described in terms of an effective magnetic anisotropy K_a, resulting from the interplay of magnetocrystalline, magnetoelastic and shape anisotropies, together with the magnetostatic interaction energy density between nanowires in the array. The experimentally determined coercive fields are compared with results of micromagnetic calculations, performed considering the magnetization reversal mode acting in each studied array and microstructure parameters. A method is proposed to roughly estimate the value of K_a experimentally, from the hysteresis loops measured at different temperatures. These measured values are in agreement with theoretical calculations. The observed temperature dependence of coercivity does not arise from an intrinsic property of pure Ni but from the nanowires surface roughness and the way the array is measured, with or without the alumina template and/or the aluminum support.

1. Introduction

During the last decades, magnetic metallic nanowires attracted increasing interest among nanometer-sized materials due to their potential applications in different fields. These nanostructures are also of scientific interest because many physical properties are significantly enhanced when two dimensions are reduced down to the nanometer scale. In ferromagnetic wires, the cylindrical geometry induces an easy axis along the major nanowire axis, resulting in a strong shape anisotropy, which may compete and even overpass the other anisotropies contributions, such as the magnetocrystalline and the magnetoelastic ones.

The hysteresis behavior of ferromagnetic Ni nanowire (NW) arrays, grown by electrodeposition inside the pores of anodic aluminum oxide (AAO) templates, has been extensively studied [1–11]. The array properties depend on the structure of the individual wires, the dipolar interactions between these wires and also on the extent of the mechanical interaction between the Al substrate, the alumina template and the metallic nanowires, arising from internal thermal stresses and the large magnetostriction of Ni. The important microstructural features of individual nanowires are their composition, crystallinity, the mean grain size, the crystallographic texture (if any), their shape and size, and the surface morphology.

NW's growth by electrodeposition can be obtained using either alternating or direct current (AC or DC, respectively). According to the parameters used in each technique, different nanowire morphologies can be synthesized: they can be smooth and uniform or dendritic-like, with many branches and surface defects; they can be polycrystalline with no preferred orientation or strongly textured [10,12–14].

Even when Ni nanowires arrayed into alumina pores have been extensively studied, a detailed analysis of the magnetic properties of these arrays as a function of temperature has not yet been fully addressed. As temperature increases in the range between 5 K and 300 K, a monotonic reduction in coercivity is observed in bulk multidomain Ni

* Corresponding author.
E-mail address: bercoff@famaf.unc.edu.ar (P.G. Bercoff).

https://doi.org/10.1016/j.cap.2018.06.014
Received 22 March 2018; Received in revised form 15 June 2018; Accepted 26 June 2018
Available online 10 July 2018

ferromagnets [15], and in regular pure Ni nanowires grown inside porous alumina when measured without the aluminum substrate [16]. A similar behavior is found in pure single-domain Ni nanoparticles [17], Ni films [18], and also in arrays of nanowires with relatively large diameters ($\geq$90 nm) as observed in Ref. [19]. This decrease in coercivity with increasing T is also frequently found in thick smooth nanowires measured with and without the aluminum substrate.

However, some studies in the temperature range between 5 K and 300 K [20–23] coincide in that arrays of thin nanowires measured inside the alumina template, exhibit a maximum in the coercive and anisotropy fields around room temperature, a behavior that cannot be rationalized by shape anisotropy considerations only. The shape anisotropy term in the magnetic energy of each nanowire promotes a uniaxial anisotropy along the wire (easy axis normal to the alumina template plane). During cooling, only a slight increase in this energy density is expected due to increasing saturation polarization.

It has long been known that the magnetocrystalline energy constants K_1, K_2 and K_3 in bulk pure Ni strongly depend on temperature in the range 4.2 K–300 K [24]. However, their complex behaviors cannot explain the increase in coercivity with temperature. Then, this phenomenon is not due to an intrinsic property of nanostructured pure Ni nor to a low dimensionality effect or to the ordered nature of the arrays. To explain this coercive field maximum at room temperature, it has been proposed [20,21] that the effective easy magnetization axis could change from parallel to perpendicular to the Ni nanowire axis as temperature decreases. The axis rotation is explained by the competition between the shape easy axis (parallel to the wire axis) and the magnetoelastic easy plane, normal to the wire axis. Shape anisotropy weakly depends on temperature through the magnetization $M(T)$. On the contrary, magnetoelastic anisotropy induced by thermal stresses (arising from the mismatch of thermal expansion coefficients of Al, alumina and Ni), is quite sensitive to changes in temperature through Ni magnetostriction, which is dependent on the temperature.

In this work, we explore the coercive field vs. temperature relationship in the range between 5 K and 300 K for pure Ni NWs arrays, in three different scenarios. To realize these conditions we synthesize Ni NWs by AC and DC electrodeposition to obtain distinct surface morphologies (smooth and rough). Two types of AAO templates with three pore sizes were selected to produce arrays of different diameters. The Al substrate was not dissolved in the template used for AC deposition. The magnetic hysteresis properties of the arrays are determined, with special attention to the temperature dependence of the effective anisotropy in each array. Using micromagnetic models, effective anisotropy constants are estimated for the three different systems as a function of microstructure variables and temperature. We propose a method to estimate this effective constant through experimental measurements and compare the results with those corresponding to calculations, obtaining a good agreement. These results indicate that surface irregularities and roughness play a crucial role in the room temperature coercivity maximum observed in some Ni nanowire arrays.

2. Experimental procedures

The templates with smaller pore diameters (shown in Fig. 1a and referred to as “home-made” hereafter) were prepared in our lab, following a well-known two-step procedure [25], as described in Refs. [5,26].

After anodization, the templates used for AC deposition were immersed in a H_3PO_4 5% v/v solution at room temperature (RT) for a short time, in order to thin the barrier layer and widen the pores' diameter while keeping the aluminum substrate. Alternatively, the remaining aluminum substrate was completely removed from the templates used for DC deposition in a 1 M $CuSO_4$ solution. An etching treatment with H_3PO_4 5% v/v solution was later performed in order to remove the barrier layer. Finally, a 50 nm Au layer was sputtered on the bottom of the template, to provide electrical contact.

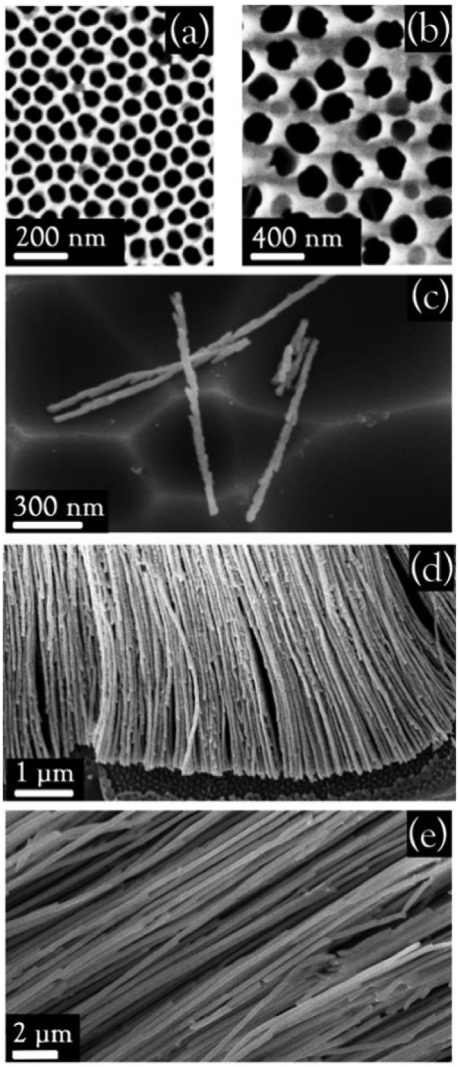

Fig. 1. SEM images of (a) home-made and (b) commercial templates. Nanowire arrays corresponding to samples (c) AC33, (d) DC65 and (e) DC200.

Commercial templates of 200 nm pores' diameter were provided by Whatman© (Fig. 1b). These templates exhibit a larger dispersion in diameter and in the nanopore hexagonal ordering (the interpore distance) than the home-made templates.

The template's geometry is usually characterized by the pore's diameter (d) and the center-to-center distance of neighboring pores (dcc). The template's porosity (P) can be analytically calculated [4] from these parameters, using the relation $P = \frac{\pi}{2\sqrt{3}}\left(\frac{d}{dcc}\right)^2$.

Both AC and DC electrodepositions were conducted at RT, using similar electrolytes: (nickel sulfate) 60 g/l $NiSO_4{\cdot}6H_2O$ + 40 g/l H_3BO_3 or (nickel sulfamate) 515 g/l $Ni(H_2NSO_3)_2{\cdot}4H_2O$ + 20 g/l $NiCl_2{\cdot}6H_2O$ + 20 g/l H_3BO_3. The resulting pH was 3–4 in both cases.

AC electrodeposition was performed using home-made templates with thinned barrier layer and keeping the aluminum substrate. A carbon rod and the Al substrate were used as electrodes, with root-mean-square voltage V_{rms} = 16 V, frequency f = 200 Hz and electrodeposition time t_{ED} = 1.5 min. The electrolyte was previously stirred with highly pure nitrogen.

DC electrodeposition was performed in an Autolab 302 N equipment with a three-electrode cell, using commercial and home-made (H-m) templates, with Au substrate. A carbon rod, the template and an Ag/AgCl 3 M KCl electrode were used as the counter-electrode, working-

Table 1
Experimental conditions for Ni NWs electrodeposition inside the pores of home-made (H-m) and commercial alumina templates. DC or AC potential, with a frequency f and a root-mean-square V, were applied during a deposition time t_{ED}.

Sample	Template	Electrolyte	Method	V [V]	f [Hz]	t_{ED} [min]
AC33	H-m	Nickel sulfate	AC	16.0 ± 0.1	200	1.5
DC65	H-m	Nickel sulfate	DC	−1.20 ± 0.02	–	15
DC200	Whatman©	Nickel sulfamate	DC	−1.20 ± 0.02	–	10

electrode and reference-electrode, respectively. A voltage $V = -1.2$ V was applied to all samples, and electrodeposition time t_{ED} was adjusted to control the nanowires' length. The electrolyte was stirred with highly pure nitrogen during the electrodeposition process. Table 1 lists the electrodeposition conditions for the selected samples.

A Sigma Zeiss Field Emission - Scanning Electron Microscope (FE-SEM), with an Oxford Energy Dispersive Spectrometer (EDS) was used to determine the samples' morphology and chemical composition (LAMARX facilities). Crystalline structures were determined by X-ray diffraction (XRD) in a Philips PW 1800/10 diffractometer with Cu K_α radiation ($\lambda = 1.540$ Å). Magnetic hysteresis loops were measured in a Super Conducting Quantum Interference Device (SQUID) in the 5 K–300 K temperature range.

Table 2 displays the main parameters that characterize the three systems under study.

3. Results and discussion

3.1. Morphologies and microstructures

From several SEM images, the nanowires' length (L) and aspect ratio a_r ($a_r = L/d$) were determined (see Table 2). Selected SEM images illustrating the templates used and the morphology of each NW array are shown in Fig. 1. All wires exhibit an overall cylinder-like shape with large aspect ratios and different morphologies. Nanowires DC200 are relatively regular, with some bifurcations but with little surface rugosity. On the contrary, nanowires AC33 exhibit a ramified morphology, with marked lateral branches making very irregular surfaces along the wires. Sample DC65 represents a condition with an intermediate density of small branches. This irregular shape has also been reported by Zeng et al. [20], who noticed that significant branching appears for low anodization voltages, when the alumina pore walls are at the time more porous. As already stated by these authors, the cause of the branching is not completely clear due to the complicated mechanisms involved in pore development in the Al support. These small branches are thought to develop inside the lateral voids in the pore wall.

EDS analysis was performed on all the samples. The spectra indicate that the wires are mainly composed of pure nickel with some traces of aluminum and oxygen from the template, on the surface. Fig. 2 (a) shows an X-ray map of sample DC200, which is representative of the other samples, where some Al remaining from the AAO (blue) can be seen on the Ni (yellow) NW. The EDS spectrum corresponding to the whole area is shown in Fig. 2(b).

Table 2
Geometric parameters of Ni NW arrays. Wire diameter d and length L lead to high aspect ratios a_r. The mean inter-pore distance dcc and the template porosity P are also listed.

Sample	d [nm]	dcc [nm]	L [μm]	a_r	P [%]
AC33	33 ± 3	55 ± 6	1.5 ± 0.2	45 ± 7	33 ± 9
DC65	65 ± 5	104 ± 7	5 ± 1	80 ± 20	35 ± 7
DC200	200 ± 40	290 ± 40	10 ± 1	50 ± 10	40 ± 10

Bulk nickel materials crystallize in a face-centered-cubic (*fcc*) structure, and many studies find that nanostructured Ni materials also have this structure [26–29]. XRD measurements were performed on samples AC33, DC65 and DC200, and Fig. 3 shows the results. A *fcc* Ni phase [PDF 00-004-0850] is confirmed in all cases, with peaks indexed at 44.91° (111), 52.05° (200), 76.57° (220) and 93.24° (311) in 2θ. The background contribution is noticed in the diffractograms: Al substrate for AC33 and SiO_2/Si wafer for DC65. The amorphous Al_2O_3 template is specially noticed in sample DC200.

All wires are polycrystalline; a rough estimation of the crystallite size using the Scherrer formula, leads to $d_{Sch} = (30 \pm 10)$ nm for samples DC65 and DC200, and $d_{Sch} = (20 \pm 10)$ nm for AC33. This indicates that for DC deposition, above a certain radius the crystallization mechanism of Ni is not sensitive to the pore diameter. Regarding crystallographic texture, sample DC200 is textured in the [220] direction, while no conclusive results may be obtained for DC65 and AC33 due to extensive overlap with the Al and Si peaks. However, in these cases the external wire morphology strongly suggests that grains are preferentially oriented.

3.2. Magnetic properties

Two configurations were considered for measuring the magnetic properties of the NWs embedded in the templates, parallel (PA) and perpendicular (PE) orientations, with respect to the relative angle between the wires' main axis and the applied field direction. Working temperatures T were chosen in the range from 5 K to 300 K.

Low-temperature measurements are interesting because some effects become relevant in this range, like a high magnetostriction [30,31] and a strong magnetocrystalline anisotropy [32].

Magnetic hysteresis loops were performed with a maximum applied field of 2 T, reaching magnetic saturation in all cases. Fig. 4(a–c) show the hysteresis loops at 300 K, in PA and PE configurations. These loops were modified from the originals, by subtracting a linear contribution arising from the substrate (Al, Au) and the diamagnetic contributions from the alumina template.

The difference between PA and PE behavior indicates the extent of the shape anisotropy contribution in each array: sample DC200 is magnetically very soft and the two loops are quite similar, indicating that the effective anisotropy K_a is very low. For AC33 and DC65 there is clearly an effective longitudinal anisotropy (parallel to the wires axes).

Hysteresis loops were measured at $T = 5$, 20, 50, 100, 200 and 300 K and the resulting coercive field values $\mu_0 H_C$ are shown in Fig. 5(a) as function of temperature, for the three arrays in PA configuration. Fig. 5(b) depicts the saturation magnetization M_S relative to the value at 5 K.

In sample DC200, coercivity decreases as temperature increases. On the contrary, an unexpected behavior of $\mu_0 H_C$ is observed in arrays with small diameters, AC33 and DC65, in which coercivity increases with T. Besides, at low temperatures, $\mu_0 H_C$ goes through an inflexion point at about 50–100 K, while sample DC200 slightly decreases for increasing T. As indicated before, similar results in Ni NW systems with granular structure and irregular surfaces were observed by other authors [5,20–22].

The increase of coercivity with increasing T for Ni NWs has been addressed by other authors [20–22,31,33,34] in terms of an effective magnetic anisotropy resulting from the interplay of magnetocrystalline (K_{mc}), magnetoelastic (K_{me}) and shape (K_{sh}) anisotropies. The magnetostatic interaction energy density (K_{int}) must also be considered. The dipolar interactions between the wires can be modeled with a mean-field approach [3,35] as an effective uniaxial anisotropy field oriented perpendicular to the wire axis and proportional to the saturation polarization and the template's porosity. As the porosities are similar within 5% in the three geometric configurations investigated in this work, no differential effects of this term on the magnetic behavior are

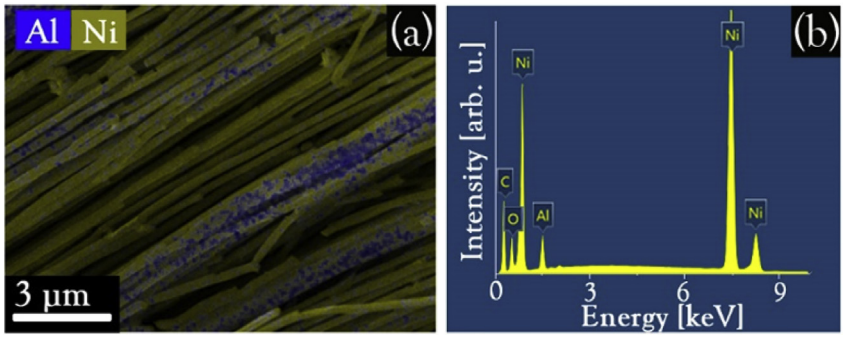

Fig. 2. (a) X-ray map of sample DC200. Ni (yellow) is the main component and some Al (blue) remains from the template can be seen. (b) EDS spectrum corresponding to this sample. (For interpretation of the references to colour in this figure legend, the reader is referred to the Web version of this article.)

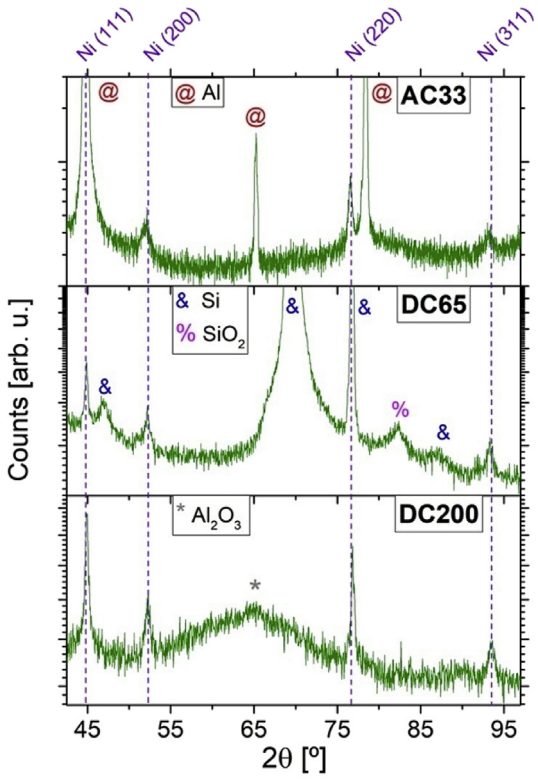

Fig. 3. XRD measurements of samples AC33, DC65 and DC200. Fcc Ni phase is confirmed in every case. There are some extra contributions from the substrate or background for each sample: Al substrate for AC33, SiO_2/Si wafer for DC65 and Al_2O_3 template for DC200.

expected.

Then, the temperature dependence of $\mu_0 H_C$ results from the variation of the effective anisotropy with temperature. The magnitudes contributing to this effective anisotropy are $K_{me} = 3\lambda\sigma/2$ with λ and σ the magnetostriction and the misfit thermal stress, respectively; $K_{sh} = \frac{1}{2}\mu_0 M_S^2 \Delta N \cong \frac{1}{4}\mu_0 M_S^2 [1 - 3N_Z(L)]$ with $N_Z(L)$ the demagnetizing factor in the long wire axis direction; $K_{mc} = \frac{2}{9}(3K_1 + K_2)$, with K_1 and K_2 the Ni anisotropy constants which strongly depend on temperature; and $K_{int} \approx -2\mu_0 M_S^2 P$, being P the porosity of the alumina template [4]. This value of K_{int} is actually an upper bound resulting for an ideal filling factor. Then, the coercive field as a function of temperature may be expressed as:

$$\mu_0 H_C(T) = \frac{2K_{mc}(T)}{M_S(T)} + \frac{3\lambda(T)\sigma(T)}{M_S(T)} + \frac{1}{2}[1 - 3N_Z(L)]\mu_0 M_S(T) - 4P\mu_0 M_S(T) \quad (1)$$

Assuming that shape anisotropy is the leading term in the entire temperature range, this expression may be rearranged as:

$$\mu_0 H_C(T) = \mu_0 H_{sh}(T) + N_{eff}(T)\mu_0 M_S(T) \quad (2)$$

with

$$N_{eff}(T) = \frac{2}{\mu_0 M_S^2(T)}[K_{mc}(T) + K_{me}(T) + K_{int}(T)] = \frac{2K_a(T)}{\mu_0 M_S^2(T)}, \quad (3)$$

and $\mu_0 H_{sh}(T) = \frac{1}{2}[1 - 3N_Z(L)]\mu_0 M_S(T)$.

In this picture, the effective demagnetizing factor N_{eff} results directly proportional to an effective anisotropy energy density K_a (T), accounting for the observed variation of the easy axis direction, relative to the nanowire long axis, as the temperature changes. Positive values of $K_a(T)$ reinforce the easy axis in the longitudinal direction while negative values indicate a competition with shape anisotropy, promoting the deviation of the easy axis to a direction normal to the long wire axis.

This variation in the easy axis direction as temperature changes may be roughly estimated by considering the relationship between the

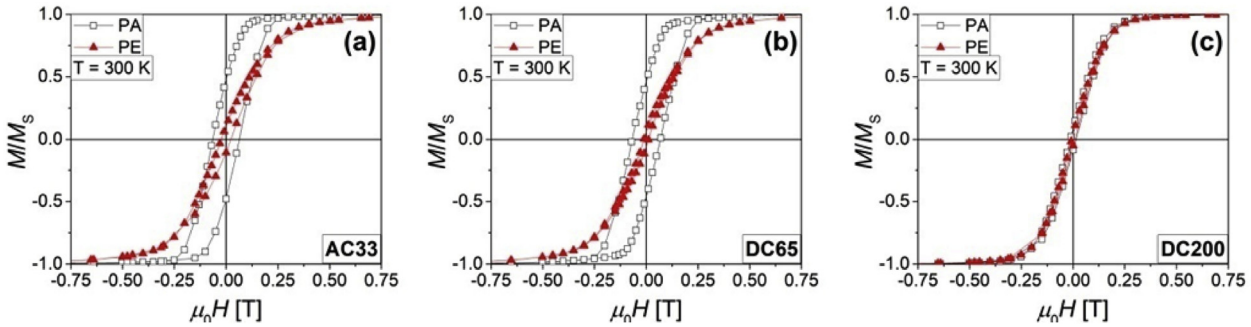

Fig. 4. Room temperature (T = 300 K) hysteresis loops for samples (a) AC33, (b) DC65 and (c) DC200. Paramagnetic and diamagnetic contributions have been subtracted.

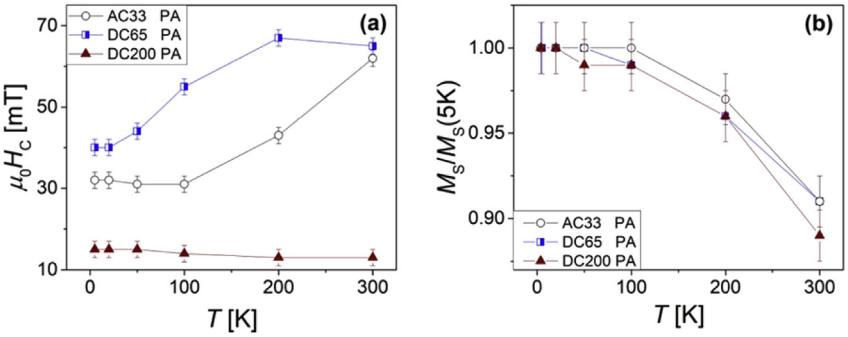

Fig. 5. Magnetic hysteresis properties as function of temperature in PA configuration: (a) coercivity and (b) normalized saturation magnetization. In samples AC33 (open circles) and DC65 (squares) coercivity increases with increasing temperature.

effective demagnetizing factor and the slope of the hysteresis loop [36]:

$$\frac{B_i}{\mu_0} = \frac{1}{N}H_{app} - \frac{1-N}{N}H_i,$$

where $B_i = \mu_0(H_i + M)$ and $H_i = H_{app} - NM$, with H_{app} the applied field and N the sample geometric demagnetizing factor. For $H_i = 0$, at the origin of the hysteresis loop ($H_{app} = 0$, $M = 0$), this line has a slope. $dM(T)/dH_{app} \propto \left|\frac{1}{N(T)}\right|$ which may be roughly approximated by the slope of the hysteresis loop (differential susceptibility) near coercivity, $\left.\frac{dM(T)}{dH_{app}}\right|_{H_{app}=H_C}$, at each temperature.

Then, the experimental slopes using $\mu_0 M_S = 0.61$ T (the Ni saturation polarization), in both PA and PE configurations, can be associated to the magnitude of the effective demagnetizing factor value N_{eff} at each temperature:

$$N_{eff}(T) = \frac{1}{\left[\left.\frac{dM(T)}{dH}\right|_{H=H_C}\right]_{exp}} = \frac{2K_a(T)}{\mu_0 M_S^2(T)} \quad (4)$$

The top panel of Fig. 6 displays the maximum slope of the hysteresis loops of sample AC33 (left) and DC65 (right).

It is clear from these results that for high temperatures, the easy axis is the longitudinal nanowire axis, while below a critical temperature (which is higher for the thinner wires) the easy axis rotates towards the plane perpendicular to the long axis. A strong dependence of K_a on temperature is expected to account for this behavior.

Taking from Fig. 6 (Top panel) representative values of the experimental slope $d(M/M_S)/d(\mu_0 H)$ for PA configuration in AC33, about 8 1/T, the corresponding demagnetizing factor is 0.20–0.16, leading to values of $|K_a(T)|\left(=\frac{1}{2}N_{eff}(T)\mu_0 M_S^2(T)\right)$ of (30–24) kJ/m^3.

In order to explore the influence of thermal activation processes on the magnetization reversal mechanism of these samples, M vs T curves were measured following the ZFC-FC protocol (see insets in the central panel of Fig. 6). It is known [37] that the profile of the d(M_{ZFC} - M_{FC})/dT curve is indicative of the energy barrier distribution (shape, center and width) corresponding to the thermally activated magnetization processes in the sample at different temperatures; these profiles are shown in the central panel of Fig. 6 for AC33 (left) and DC65 (right) for PA configuration. Remarkably, the distribution corresponding to sample AC33 is wider than that observed for DC65, in agreement with the irreversibility temperature above 300 K observed for AC33. This fact may be explained considering that sample AC33 exhibits extensive branching; because of this unique morphology, every branch could act as a nucleation site making the magnetization reversal initiate by numerous nucleation processes with different activation barriers. In addition, different nanowires may also have distinct activation barriers leading to a wide distribution of nucleation fields. Then, it is not likely that a single-energy-barrier picture can be used to describe such a system.

On the contrary, the activation barrier distribution in DC65 is quite narrow, suggesting that nucleation events may be well described by a single thermally-activated process. This may be due to the lesser extent of branching in DC65 nanowires. The roles of magnetocrystalline and magnetoelastic contributions in the effective anisotropy controlling magnetization reversal are discussed at the end of this section.

As previously indicated, the coercive fields clearly increase with

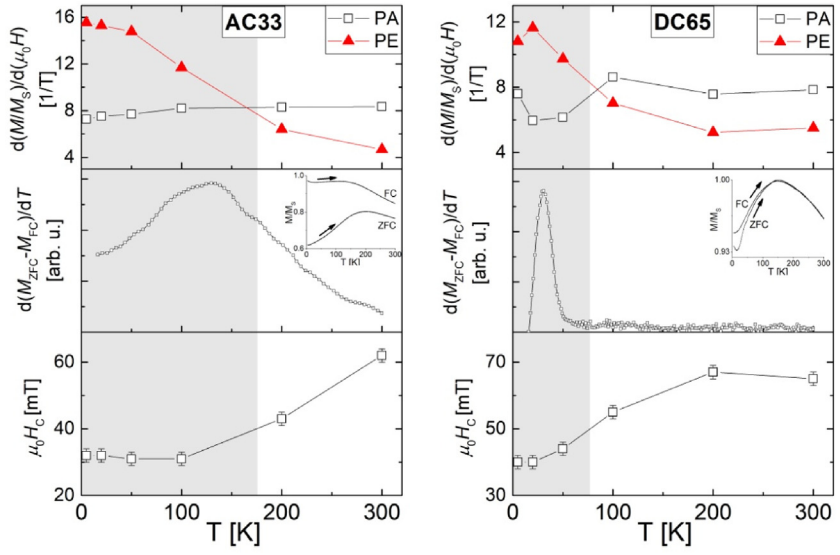

Fig. 6. Top panel (left: AC33; right: DC65): Maximum slope of the M/M_S *vs.* $\mu_0 H$ curves in PA (open squares) and PE (solid triangles) configurations as a function of temperature. Central panel: Energy barriers distribution profile, calculated as the derivative d(M_{ZFC}-M_{FC})/dT in the PA condition. The inset shows the M/M_S vs T curve, measured in ZFC and FC modes. Bottom panel: Coercivity values as a function of temperature, for the PA configuration.

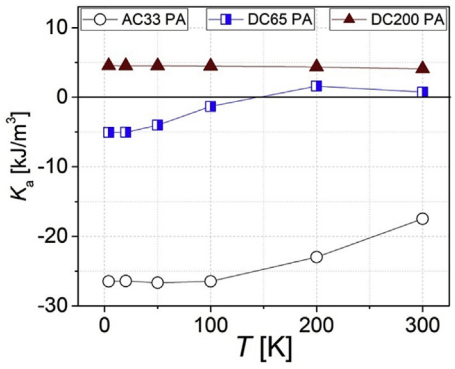

Fig. 7. Effective anisotropy K_a as a function of temperature T. Sample AC33 (open circles) has a negative value for K_a in the whole temperature range, while for sample DC200 (solid triangles) K_a is always positive. Sample DC65 (half-open squares) has a dual behavior: the effective anisotropy is negative for temperatures up to 140 K, and it is positive above this value.

temperature above 50–100 K. A possible explanation for this behavior considers that, even when the shape anisotropy is appreciable, the easy axis direction is not constant during measurement. In fact, the relative saturation magnetization *vs.* temperature $M_S(T)$ shown in Fig. 5(b) indicates that this magnitude does not change much in the measurement range.

3.2.1. Magnetization reversal models

It is accepted [38,39] that in Ni nanowires with diameters larger than the exchange length $l_{ex} = (2\ A/\mu_0\ M_S^2)^{1/2}$ ($l_{ex} = 9.9$ nm [40] at room temperature), the polarization reversal mechanism is localized. Here, $A = 9 \times 10^{-12}$ J/m is the stiffness constant [41], $\mu_0 M_S = 0.61$ T [40] is the Ni saturation polarization and M_S is Ni saturation magnetization. On the contrary, when $d < l_{ex}$, delocalized modes, such as global coherent rotation or global curling may take place. Then, localized, relatively soft and non-uniform nucleation modes are predicted for all the three samples [42–44]. Depending on the magnetic hardness and the wire diameter, these nuclei may be formed by coherent rotation (C) or by curling (V). In the first case the nucleus is bounded by a Bloch-like wall, while in the second case a vortex-like wall is created.

Escrig et al. [42–44] assumed that the nucleation field of a system that reverses its magnetization by means of the nucleation and propagation of a Bloch-like wall is equal to the nucleation field of an equivalent system with an effective volume (related to the nucleus volume) that reverses its magnetization by coherent rotation. Then, the nucleation field for the applied field parallel to the wire axis is given by [43,44]:

$$H_C^B = |H_n^B| = \frac{2[K(w_B) + K_a]}{\mu_0 M_S}, \tag{5}$$

where w_B is the Bloch-like wall thickness, which is obtained analytically by minimizing the energy described in Ref. [45], $K(w_B) = \frac{1}{4}\mu_0 M_S^2[1 - 3N_Z(w_B)]$ is the shape anisotropy constant for this process and K_a is defined in Eq. (3).

For thicker nanowires such as D200, it is expected that the magnetization reversal is originated in a local curling process [27]. The curling nucleation field in a prolate spheroid (the nucleus) was first calculated by Aharoni [46] in 1997. The effect of adding an anisotropy contribution is essentially the same as changing the shape anisotropy by modifying the aspect ratio [46]. To determine the nucleation field $H_n^V(\theta)$, Eqns. (6a) and (6b) are simultaneously solved numerically for the applied field parallel to the wire axis [46]:

$$H_n^V(0)\cos(\omega) = (N_x(L)\sin^2\omega + N_Z(L)\cos^2\omega - c - (2K_a/\mu_0 M_S^2)[3\cos^2\omega - 1])M_S \tag{6a}$$

$$-H_n^V(0)\sin(\omega) = \left(\frac{1}{2}[N_x(L) - N_Z(L) + (2K_a/\mu_0 M_S^2)]\sin(2\omega)\right)M_S \tag{6b}$$

where $c = q^2 L_{ex}^2/R^2$, q is a dimensionless parameter, $R = d/2$ is the radius of the wire and ω is the critical angle between polarization and the wire axis for an inverse domain nucleation. For a cylindrical geometry, Shtrikman and Treves [47] obtained $q^2 = 1.08\ \pi$. As pointed out by Aharoni [46], a jump of the magnetization for an isolated system occurs at or near the vortex nucleation field. Therefore, the coercivity H_C^V is quite close to the absolute value of the nucleation field, and it is possible to assume that in the vortex mode. $|H_n^V| \approx H_C^V$ is a good approximation.

3.2.2. Analytical results

NWs with small diameters (AC33 and DC65) are assumed to reverse their magnetization through the propagation of a Bloch-like domain wall of thickness w_B [48], while arrays of nanowires with larger diameter such as DC200, reverse their magnetization through the propagation of a vortex-like domain wall of thickness w_V [49].

Once the reversal mechanism is determined for each system, only one free variable is left to fit the analytical model to the coercive field experimental data. This parameter is the effective anisotropy K_a, which results, as mentioned before, from the interplay of the crystalline anisotropy of the NWs, the magnetostatic interactions in the array and the magnetoelastic anisotropy, this latter arising from the mismatch of thermal coefficients between the templates and the Ni wires.

Fig. 7 shows the effective anisotropy constant K_a as a function of temperature T calculated for the three samples under consideration, assuming in each case the selected mechanism. It may be observed that in sample AC33, K_a exhibits a negative value in the whole temperature range, indicating that it favors a magnetization perpendicular to the wires' long axis, directly competing with shape anisotropy. The resulting absolute values are relatively close to those estimated from Fig. 6 for AC33 in PA condition, (-30 to -24) kJ/m^3. On the other hand, for the sample with the largest diameter, DC200, the anisotropy constant K_a exhibits a low (and positive) value, quite constant in the entire temperature range. Small coercive field values are observed in the hysteresis loops at 300 K (see Fig. 4(d)), suggesting that in this case, shape effects are almost balanced by the other contributions to K_a.

A remarkable behavior is observed in sample DC65, for which a negative effective anisotropy is obtained (favoring an easy plane perpendicular to the wires) for temperatures between 5 K and 140 K, and a positive effective anisotropy (favoring the wires' main axis) for temperatures above 140 K. This implies that it is possible to control not only the magnitude of the anisotropy, but also the direction of the easy magnetization axis, simply by varying the temperature of the nanowire array.

The upper bound of the shape anisotropy constant, estimated assuming long perfect cylinders is about 74 kJ/m^3; the magnetocrystalline anisotropy (K_{mc}) of Ni strongly depends on temperature, K_1 changing from -4.5 to -12 kJ/m^3, and K_2 from -2.3 to 3 kJ/m^3 when the temperature changes from 300 K to 4.2 K. Then, at low temperatures, K_{mc} may become of the same order as K_{sh}. De la Torre et al. [11] reported that in quasi single-crystal wires K_{mc} increases as the wire diameter decreases. However, our nanowires are polycrystalline, with no preferential orientations, so changes in K_{mc} with temperature are not expected to determine the overall anisotropy change. Also, K_{me} monotonously increases with decreasing T, through the increase in the thermal stress σ(T), to reach values close to the ones for shape anisotropy.

Regarding magnetoelastic effects, previous studies [20–22,50] have shown that they largely influence the magnetic properties of Ni nanowires, due to a large mismatch between the thermal expansion coefficients α of Ni and alumina and between Ni and the Al serving as a substrate. At room temperature, $\alpha_{Ni} = 13.4 \times 10^{-6}\ K^{-1}$, $\alpha_{Al} = 23.8 \times 10^{-6}\ K^{-1}$ and for re-crystallized alumina

$\alpha_{Al2O3} = 6 \times 10^{-6} K^{-1}$; due to these large differences, Ni wires contract more than the alumina pores during cooling but less than the aluminum substrate, leading to an increasing tensile stress along the wire axis as the temperature decreases. This, in time, induces additional magnetoelastic anisotropy. In wires of irregular shape, their relative position to the pore wall is fixed by numerous branches, and therefore, the wires are forced to contract or expand together with the alumina wall. The interaction with the Al substrate leads to an upper bound for the magnetoelastic anisotropy.

Considering values $\lambda s \approx -34 \times 10^{-6}$ for the isotropic magnetostrictive constant and a Young's modulus for Ni of $E = 200$ GPa, the magnetoelastic anisotropy constant for sample AC33 is $K_{me} \approx -10$ kJ/m^3 at about 20 K. If the wires are irregular but the substrate is very thin (sample DC65 with Au sputtering), the magnetoelastic anisotropy is reduced to $K_{me} \approx -6.5$ kJ/m^3. In the case of smooth wires and very thin substrate (DC200 with Au sputtering), there are no significant tensile stresses and the magnetoelastic anisotropy vanishes. These estimations indicate that the maximum magnetoelastic contribution to K_a is obtained for AC33, while a lower values result for DC65 and a weak K_a is attributed for DC200.

4. Conclusion

Hysteresis properties of Ni nanowires arrays embedded in alumina templates, are determined in the range between 5 K and 300 K for three scenarios: nanowires AC33 with a rough, densely branched surface (measured with the Al substrate); DC65 with lower roughness and sparse surface branching (measured without the Al substrate); and coarse nanowires DC200, with quite smooth external surface (measured without the Al substrate). The diameters of all the nanowires investigated are larger than the limit value for uniform magnetization reversal modes ($\sim$10 nm) so localized modes operate. In all the samples a mechanism of nucleation of inverse domains and further expansion of a domain wall controls the coercivity.

The coercive field in DC200 slightly –but monotonously– decreases for increasing temperature and the polarization reversal occurs through the propagation of a vortex-like domain wall in the whole temperature range. On the other hand, the reversal mode in samples DC65 and AC33 is given by the propagation of a Bloch-like domain wall in the whole temperature range, with an effective anisotropy K_a. In these latter samples, coercivity is found to increase with temperature. This infrequent behavior is explained by the competition between shape and magnetoelastic anisotropies.

Magnetoelastic anisotropy is the highest when the arrays are measured with the alumina template and the Al support, and the wires have rough surfaces, which strongly attach the wire to the alumina wall, forcing it to expand or contract together with the pore. On the contrary, when the wire surface detaches from the wall (smooth surface), this anisotropy is vanishing small. This explains why only in branched nanowires magnetoelastic effects actually compete with shape anisotropy, leading to the easy axis rotation and the unusual increase of coercivity with temperature. It is worth noting that this effect does not arise from an intrinsic property of pure Ni but from the nanowire surface roughness and the way nanowires are measured, with or without the alumina template and/or the aluminum support.

From morphological and magnetic data, and considering the magnetization reversal mechanism previously determined, the effective anisotropy constant K_a for each sample type was calculated as a function of temperature, in the interval 5 K–300 K. It is found that in DC200 the effective anisotropy is almost constant and small (5 kJ/m^3) and always positive. In the case of sample AC33, K_a is always negative, ranging from -28 kJ/m^3 at 5 K to -18 kJ/m^3 at 300 K. A special case is found in sample DC65, where K_a is negative at low temperature and becomes positive above 140 K.

Acknowledgements

This work has been partially funded by CONICET, SECyT, UNC and ANPCyT-FonCyT, Argentina. JE acknowledges financial support from FONDECYT 1150952 and from CONICYT Proyecto Basal FB0807, Chile.

References

[1] T.M. Whitney, J.S. Jiang, P.C. Searson, C.L. Chien, Fabrication and magnetic properties of arrays of metallic nanowires, Science 261 (1993) 1316–1319.
[2] D.J. Sellmyer, M. Zheng, R. Skomski, Magnetism of Fe, Co and Ni nanowires in self-assembled arrays, J. Phys. Condens. Matter 13 (2001) R433–R460.
[3] A. Encinas-Oropesa, M. Demand, L. Piraux, I. Huynen, U. Ebels, Dipolar interactions in arrays of nickel nanowires studied by ferromagnetic resonance, Phys. Rev. B 63 (2001) 104415.
[4] K. Nielsch, F. Müller, A.P. Li, U. Gösele, Uniform nickel deposition into ordered alumina pores by pulsed electrodeposition, Adv. Mater. (Weinheim, Ger.) 12 (2000) 582–586.
[5] F. Meneses, P.G. Bercoff, Influence of the porosity on the magnetic properties of Ni nanowires arrays, Materia 20 (2015) 722–730.
[6] M. Vázquez, M. Hernández-Vélez, K. Pirota, A. Asenjo, D. Navas, J. Velázquez, P. Vargas, C. Ramos, Arrays of Ni nanowires in alumina membranes: magnetic properties and spatial ordering, Eur. Phys. J. B40 (2004) 489–497.
[7] X.W. Wang, G.T. Fei, X.J. Xu, Z. Jin, L.D. Zhang, Size-dependent orientation growth of large-area ordered Ni nanowire arrays, J. Phys. Chem. B 109 (2005) 24326–24330.
[8] R. Lavin, J.C. Denardin, J. Escrig, D. Altbir, A. Cortés, H. Gómez, Angular dependence of magnetic properties in Ni nanowire arrays, J. Appl. Phys. 106 (2009) 103903.
[9] X. Li, Y. Wang, G. Song, Z. Peng, Y. Yu, S. She, J. Li, Synthesis and growth mechanism of Ni nanotubes and nanowires, Nanoscale Res. Lett. 4 (2009) 1015–1020.
[10] K.M. Razeeb, F.M. Rhen, S. Roy, Magnetic properties of nickel nanowires: effect of deposition temperature, J. Appl. Phys. 105 (2009) 083922.
[11] J. De La Torre Medina, G. Hamoir, Y. Velázquez-Galván, S. Pouget, H. Okuno, L. Vila, A. Encinas, L. Piraux, Large magnetic anisotropy enhancement in size controlled Ni nanowires electrodeposited into nanoporous alumina templates, Nanotechnology 27 (2016) 145702.
[12] M.P. Proenca, C.T. Sousa, J. Ventura, M. Vázquez, J.P. Araujo, Ni growth inside ordered arrays of alumina nanopores: enhancing the deposition rate, Electrochim. Acta 72 (2012) 215–221.
[13] P. Wang, L. Gao, Z. Qiu, X. Song, L. Wang, S. Yang, R. Murakami, A multistep ac electrodeposition method to prepare Co nanowires with high coercivity, J. Appl. Phys. 104 (2008) 064304-064304-5.
[14] N.J. Gerein, J.A. Haber, Effect of ac electrodeposition conditions on the growth of high aspect ratio copper nanowires in porous aluminum oxide templates, J. Phys. Chem. B 109 (2005) 17372–17385.
[15] S. Hayashi, T. Huzimura, The effect of plastic deformation on the coercive force and initial permeability of nickel single crystals, Trans. JIM 5 (1964) 127–131.
[16] H. Zeng, R. Skomski, L. Menon, Y. Liu, S. Bandyopadhyay, D.J. Sellmyer, Structure and magnetic properties of ferromagnetic nanowires in self-assembled arrays, Phys. Rev. B 65 (2002) 134426.
[17] F.C. Fonseca, G.F. Goya, R.F. Jardim, R. Muccillo, N.L.V. Carrefio, E. Longo, E.R. Leite, Magnetic properties of Ni nanoparticles embedded in amorphous SiO2, Mater. Res. Soc. Symp. Proc. 746 (2003) 213–218.
[18] M. Hanson, C. Johansson, Temperature dependence of hysteresis loops of Ni films-characteristics of fine-grained structure, in: G.C. Hadjipanayis (Ed.), Magnetic Hysteresis in Novel Magnetic Materials. NATO ASI Series (Series E: Applied Sciences), vol. 338, Springer, Dordrecht, 1997.
[19] N. Adeela, K. Maaz, U. Khan, S. Karim, M. Ahmad, M. Iqbal, S. Riaz, X.F. Han, M. Maqbool, Fabrication and temperature dependent magnetic properties of nickel nanowires embedded in alumina templates, Ceram. Int. 41 (2015) 12081–12086.
[20] H. Zeng, S.A. Michalski, R.D. Kirby, D.J. Sellmyer, L. Menon, S. Bandyopadhyay, Effects of surface morphology on magnetic properties of Ni nanowire arrays in self-ordered porous alumina, J. Phys. Condens. Matter 14 (2002) 715–721.
[21] A. Kumar, S. Fähler, H. Schlörb, K. Leistner, L. Schultz, Competition between shape anisotropy and magnetoelastic anisotropy in Ni nanowires electrodeposited within alumina templates, Phys. Rev. B 73 (2006) 064421.
[22] D. Navas, K.R. Pirota, P. Mendoza Zelis, D. Velázquez, C.A. Ross, M. Vázquez, Effects of the magnetoelastic anisotropy in Ni nanowire arrays, J. Appl. Phys. 103 (2008) 07D523.
[23] A. Michel, A.C. Niemann, T. Boehnert, S. Martens, J.M. Montero Moreno, D. Goerlitz, R. Zierold, H. Reith, V. Vega, V.M. Prida, A. Thomas, J. Gooth, K. Nielsch, Temperature gradient-induced magnetization reversal of single ferromagnetic nanowires, J. Phys. D Appl. Phys. 50 (2017) 494007.
[24] C.R.J. Cadsden, H. Heath, The first three anisotropy constants of Nickel, Solid State Commun. 20 (1976) 951–952.
[25] H. Masuda, K.S. Fukuda, Ordered metal nanohole arrays made by a two-step replication of honeycomb structures of anodic alumina, Science **268** (1995) 1466–1468.
[26] M.S. Viqueira, S.E. García, S.E. Urreta, G.P. López, L.M. Fabietti, Hysteresis properties of hexagonal arrays of FePd nanowires, IEEE Trans. Magn. 49 (2013) 4498–4501.
[27] E. Vilanova Vidal, Y.P. Ivanov, H. Mohammed, J. Kosel, A detailed study of

magnetization reversal in individual Ni nanowires, Appl. Phys. Lett. 106 (2015) 32403.
[28] F. Tian, Z.P. Huang, L. Whitmore, Fabrication and magnetic properties of Ni nanowire arrays with ultrahigh axial squareness, Phys. Chem. Chem. Phys. 14 (2012) 8537–8541.
[29] S. Chu, K. Wada, S. Inoue, S. Todoroki, Fabrication and characteristics of ordered Ni nanostructures on glass by anodization and direct current electrodeposition, Chem. Mater. 14 (2002) 4595–4602.
[30] R.R. Birss, E.W. Lee, The saturation magnetostriction constants of nickel within the temperature range - 196° to 365°C, Proc. Phys. Soc. 76 (1960) 502–506.
[31] J. De La Torre Medina, M. Darques, L. Piraux, Strong low temperature magnetoelastic effects in template grown Ni nanowires, J. Phys. D Appl. Phys. 41 (2008) 032008.
[32] R.M. Bozorth, Ferromagnetism, D. Van Nostrand Company Inc., New York, 1951.
[33] L.G. Vivas, M. Vázquez, V. Vega, J. García, W.O. Rosa, R.P. del Real, V.M. Prida, Temperature dependent magnetization in Co-base nanowire arrays: role of crystalline anisotropy, J. Appl. Phys. 111 (2012) 07A325.
[34] C. Bran, E.M. Palmero, Zi-An Li, R.P. del Real, M. Spasova, M. Farle, M. Vázquez, Correlation between structure and magnetic properties in Co_xFe_{100-x} nanowires: the roles of composition and wire diameter, J. Phys. D Appl. Phys. 48 (2015) 145304.
[35] F. Zighem, T. Maurer, F. Ott, G. Chaboussant, Dipolar interactions in arrays of ferromagnetic nanowires: a micromagnetic study, J. Appl. Phys. 109 (2011) 013910.
[36] R.C. O'Handley, Modern Magnetic Materials: Principles and Applications, John Wiley & Sons, Inc, New York, 2000 (pg. 40).
[37] M. Knobel, L.M. Socolovsky, J.M. Vargas, Propiedades magnéticas y de transporte de sistemas nanocristalinos: conceptos básicos y aplicaciones a sistemas reales, Rev. Mexic. Fisica E 50 (2004) 8–28.
[38] R. Skomski, H. Zeng, D.J. Sellmyer, Incoherent magnetization reversal in nanowires, J. Magn. Magn. Mater. 249 (2002) 175–180.
[39] R. Skomski, H. Zeng, M. Zheng, D.J. Sellmyer, Magnetic localization in transition-metal nanowires, Phys. Rev. B 62 (2000) 3900–3904.
[40] G. Bertotti, Hysteresis in Magnetism, Academic Press, New York, 1998.
[41] A. Michels, J. Weissmüller, A. Wiedenmann, J.G. Barker, Exchange-stiffness constant in cold-worked and nanocrystalline Ni measured by elastic small-angle neutron scattering, J. Appl. Phys. 87 (2000) 5953–5955.
[42] J. Escrig, R. Lavín, J.L. Palma, J.C. Denardín, D. Altbir, A. Cortés, H. Gómez, Geometry dependence of coercivity in Ni nanowire arrays, Nanotechnology 19 (2008) 75713.
[43] J. Escrig, J. Bachmann, J. Jing, M. Daub, D. Altbir, K. Nielsch, Crossover between two different magnetization reversal modes in arrays of iron oxide nanotubes, Phys. Rev. B 77 (2008) 214421.
[44] J. Escrig, M. Daub, P. Landeros, K. Nielsch, D. Altbir, Angular dependence of coercivity in magnetic nanotubes, Nanotechnology 18 (2007) 445706.
[45] P. Landeros, S. Allende, J. Escrig, E. Salcedo, D. Altbir, Reversal modes in magnetic nanotubes, Appl. Phys. Lett. 90 (2007) 102501.
[46] A. Aharoni, Angular dependence of nucleation by curling in a prolate spheroid, J. Appl. Phys. 82 (1997) 1281–1287.
[47] S. Shtrikman, D. Treves, In Magnetism, G.T. Rado and H. Suhl. Academic: New York, 1963. Vol. 3.
[48] R. Hertel, Micromagnetic simulations of magnetostatically coupled Nickel nanowires, J. Appl. Phys. 90 (2001) 5752.
[49] E. Vilanova Vidal, Y.P. Ivanov, H. Mohammed, J. Kosel, A detailed study of magnetization reversal in individual Ni nanowires, Appl. Phys. Lett. 106 (2015) 32403.
[50] N. Ahmad, J.Y. Chen, W.P. Zhou, D.P. Liu, X.F. Han, Magnetoelastic anisotropy induced effects on field and temperature dependent magnetization reversal of Ni nanowires and nanotubes, J. Supercond. Nov. Magn. 24 (2011) 785–792.